Astronomy & Astrophysics

Chemical abundances of the metal-poor horizontal-branch stars CS 22186-005 and CS 30344-033[⋆]

Ş. Çalışkan[1], E. Caffau[2], P. Bonifacio[2], N. Christlieb[3], L. Monaco[4], T. C. Beers[5,6], B. Albayrak[1], and L. Sbordone[7,8,3]

1 Department of Astronomy and Space Sciences, Ankara University, 06100 Tandoğan, Ankara, Turkey
  e-mail: seyma.caliskan@science.ankara.edu.tr
2 GEPI, Observatoire de Paris, CNRS, Université Paris Diderot, Place Jules Janssen, 92190 Meudon, France
  e-mail: [Elisabetta.Caffau; Piercarlo.Bonifacio]@obspm.fr
3 Zentrum für Astronomie der Universität Heidelberg, Landessternwarte, Königstuhl 12, 69117 Heidelberg, Germany
  e-mail: n.christlieb@lsw.uni-heidelberg.de
4 European Southern Observatory, Casilla 19001 Santiago, Chile
  e-mail: lmonaco@eso.org
5 National Optical Astronomy Observatory, Tucson, AZ 85719, USA
  e-mail: beers@noao.edu
6 JINA: Joint Institute for Nuclear Astrophysics, Michigan State University, East Lansing, MI 48824, USA
7 Millennium Institute of Astrophysics, Av. Vicuna Mackenna 4860, 782-0436 Macul, Santiago, Chile
  e-mail: lsbordon@astro.puc.cl
8 Pontificia Universidad Católica de Chile, Av. Vicuna Mackenna 4860, 782-0436 Macul, Santiago, Chile

ABSTRACT

We report on a chemical-abundance analysis of two very metal-poor horizontal-branch stars in the Milky Way halo: CS 22186-005 ([Fe/H] = −2.70) and CS 30344-033 ([Fe/H] = −2.90). The analysis is based on high-resolution spectra obtained at ESO, with the spectrographs HARPS at the 3.6 m telescope, and UVES at the VLT. We adopted one-dimensional, plane-parallel model atmospheres assuming local thermodynamic equilibrium. We derived elemental abundances for 13 elements for CS 22186-005 and 14 elements for CS 30344-033. This study is the first abundance analysis of CS 30344-033. CS 22186-005 has been analyzed previously, but we report here the first measurement of nickel (Ni; Z = 28) for this star, based on twenty-two Ni I lines ([Ni/Fe] = −0.21 ± 0.02); the measurement is significantly below the mean found for most metal-poor stars. Differences of up to 0.5 dex in [Ni/Fe] ratios were determined by different authors for the same type of stars in the literature, which means that it is not yet possible to conclude that there is a real intrinsic scatter in the [Ni/Fe] ratios. For the other elements for which we obtained estimates, the abundance patterns in these two stars match the Galactic trends defined by giant and turnoff stars well. This confirms the value of horizontal-branch stars as tracers of the chemical properties of stellar populations in the Galaxy. Our radial velocities measurements for CS 22186-005 differ from previously published measurements by more than the expected statistical errors. More measurements of the radial velocity of this star are encouraged to confirm or refute its radial velocity variability.

Key words. stars: abundances – stars: Population II – Galaxy: abundances – Galaxy: evolution

1. Introduction

In most instances (except in cases of, e.g., pollution from a binary companion) the atmospheres of stars are expected to reflect the chemical composition of the interstellar medium from which they were born, hence, metal-poor stars provide "archaeological evidence" that constrains the early epochs of star formation in our Galaxy, see, however, Hattori et al. (2014). These stars thus play important roles in understanding the nature of the first objects that formed in the Universe; their chemical abundances can be used to infer the first few steps of Galactic chemical evolution.

Among the possible tracer populations of the very metal-poor component(s) of the Galactic halo, horizontal-branch (HB) stars have received much less attention than giant-branch (GB) or main-sequence turnoff (MSTO) stars. However, in recent years a significant number of HB stars have been subject to detailed chemical analyses (Preston et al. 2006; For & Sneden 2010; For et al. 2011; Hansen et al. 2011). These studies have shown that except for Li and C (which can be readily altered during a star's ascent of the red giant branch, RGB), these stars are indeed reliable fossil records of the material from which they formed. The HB stars are more luminous than the MSTO stars and can thus be used to probe the Galaxy to larger distances. With respect to GB stars, HB stars have the clear advantage that their masses can be derived more accurately from their surface gravities and effective temperatures through comparison with stellar evolutionary tracks.

In this paper we report on a detailed chemical-abundance analysis of two very metal-poor HB stars, one of which is analyzed here for the first time. CS 22186-005 was identified in the HK objective-prism survey of Beers et al. (1992) and was classified as an HB star by Norris et al. (1996). The abundance analysis of this star was performed by Preston et al. (2006) and For & Sneden (2010). Broadband photometric data for CS 30344-033 (rediscovered in the Hamburg/ESO survey as HE 2252-3458;

Table 1. Properties and observations log of the two program stars.

Object	RA [h m s]	Dec [° ′ ″]	B [mag]	Spectrograph	Setup	Obs. date	Exp. time [s]	λ range [Å]	Resolving power
CS 22186-005	04 13 09.1	−35 50 38.7	13.33	HARPS		March 10, 2006	2×1800	3778−6908	115 000
				UVES	blue390	November 18, 2005	3600	3280−4560	71 000
CS 30344-033	22 55 31.9	−34 42 59.0	14.61	UVES	blue390	May 28, 2006	3600	3300−4510	
					red580l	May 28, 2006	3600	4760−5800	40 000
					red580u	May 28, 2006	3600	5820−6840	

[Christlieb et al. 2008](#)) was published by [Norris et al.](#) ([1999](#)), who noted its status as a metal-weak candidate. No abundance analysis has previously been performed for this star. Section 2 describes our spectroscopic observations and data reduction, while Sect. 3 includes comments about the possible radial velocity variation of CS 22186-005. Section 4 presents details of our abundance analysis. In Sect. 5, we discuss the assignment of the evolutionary stages of these stars and their associated masses. Section 6 summarizes the results of our abundance analysis, and Sect. 7 presents a discussion of these results. We conclude in Sect. 8.

2. Spectroscopic observations and data reductions

High-resolution spectra of CS 22186-005 were obtained with two different spectrographs: the HARPS 3.6 m instrument and UVES at the VLT ([Dekker et al. 2000](#)). Two HARPS spectra ($R \sim 115\,000$), covering a wavelength range of 3778 to 6908 Å, were acquired on March 10, 2006, each with an exposure time of 1800 s. Both spectra were shifted to a rest-wavelength scale before they were combined. The spectrum of CS 22186-005, obtained with UVES, has a resolving power of $R \sim 71\,000$. It has a wavelength range of 3280−4560 Å and was acquired with 3600 s on November 18, 2005. UVES at the VLT is used to obtain high-resolution spectra of CS 30344-033. The spectra have a spectral resolution of $R \sim 40\,000$. They were acquired with 3600 s on May 28, 2006, covering a wavelength range of 3300−6840 Å. We used the pipeline-reduced spectra (as provided by the ESO data management division) retrieved from the ESO archive[1,2]. In Table 1 we list details of the observing sessions and instrumental setups as well as the coordinates and brightness of the stars, observing dates, exposure times, wavelength ranges of the spectra, and resolving powers.

As part of our reduction procedure, we rebinned the HARPS spectrum of CS 22186-005 and the UVES spectrum of CS 30344-033 by a factor of two to increase their signal-to-noise ratios (S/N). We did not apply any rebinning to the UVES spectrum of CS 22186-005, because its S/N is sufficient. We list in Table 2 the S/N ratios of each spectrum after rebinning in the wavelength regions around 4000 Å and 5000 Å. In Fig. 1, we show a portion of the final spectra in the 4225−4238 Å region for our two stars. We measured the radial velocities of the stars from the Ca II H&K lines (in the blue regions), the Mg I b lines (in the red regions), and weak iron lines over the entire wavelength ranges, as $v = c(\lambda_{obs} - \lambda_0)/\lambda_0$, where c is the speed of light and λ_0 is the rest wavelength of the line. Then we averaged
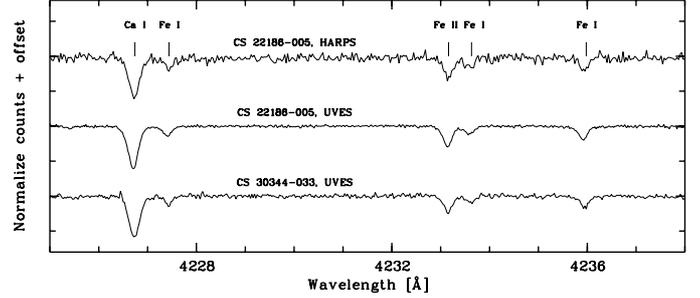

Fig. 1. The 4225−4238 Å region of the final spectra of CS 22186-005 and CS 30344-033.

the radial velocities measured from the different lines. The resulting values of the barycentric radial velocities and their errors are listed in Table 2.

3. Radial velocities: is CS 22186-005 a variable?

For CS 30344-033, our radial velocity measurement reported in Table 2 is the only one available. For CS 22186-005, however, we have two spectra, and three other measurements are available in the literature. The HARPS and UVES spectra provide two measurements that are consistent with no variation in the radial velocity, but only four months separate the two observations. From the low-resolution HK survey spectra, [Beers et al.](#) ([1992](#)) found 183 ± 10 km s^{-1} and [Beers et al.](#) ([2000](#)) 192 ± 10 km s^{-1}; given the lower precision, these measurements are consistent with ours.

[Preston et al.](#) ([2006](#)), reported 183 km s^{-1}, but did not state an error. Considering that their analysis is based on a high-quality MIKE spectrum, [Roederer et al.](#) ([2014b](#)) showed an error of $\pm 0.6 - 0.8$ km s^{-1} for the radial velocity measurements of MIKE spectra, similar to our UVES spectrum. At face value, this measurement is inconsistent with both our measurements and would be evidence for a variation in the radial velocity of the star, unless there is a large offset in measured radial velocity between MIKE and UVES, which is unlikely.

Additional monitoring of the radial velocity of this star is encouraged. If the variations in radial velocity are confirmed, it might be a binary with a very long period (given the near coincidence of the UVES and HARPS radial velocities). This would make it a very interesting object, since we could obtain an estimate of its mass independent of evolutionary tracks. The star is bright and sufficiently nearby that the *Gaia* satellite could provide an astrometric orbit if the star were a binary.

Table 2. Measured S/N ratios and barycentric radial velocities.

Object	Instrument	S/N [@4000 Å]	S/N [@5000 Å]	S/N [@6000 Å]	v_{bary} [km s^{-1}]
CS 22186-005	HARPS	16	30	40	193.6 ± 1.1
	UVES		⋯	⋯	194 ± 1
CS 30344-033	UVES	40	120	90	101.1 ± 0.6

Table 3. Stellar parameters of the targets.

Object	T_{eff} [K]	$\log g$ [cgs]	ξ [km s^{-1}]	[Fe/H]
CS 22186-005	6160	2.60	3.40	-2.70
CS 30344-033	6100	2.70	3.20	-2.90

4. Abundance analysis

4.1. Stellar parameters

For each star we started from an initial estimate of the atmospheric parameters. For CS 22186-005, we used the parameters given by For & Sneden (2010). For CS 30344-033 we used the colors given by Christlieb et al. (2008) and the calibrations of Casagrande et al. (2010) for the effective temperature. The colors in Christlieb et al. (2008) were derived from the objective prism spectra and are thus more uncertain than CCD photometry. From this temperature we used the Yale-Yonsei isochrones (Yi et al. 2003) of 10 and 12 Gyr and [Fe/H] = −2.5, [α/Fe] = +0.3 to estimate the surface gravity. With these atmospheric parameters we computed a model atmosphere using version 9 of the ATLAS code (Kurucz 1993a, 2005; Sbordone et al. 2004) using the models in the grid of Castelli & Kurucz (2003) as starting model and the same opacity distribution functions. The computation assumed local thermodynamic equilibrium (LTE), plane-parallel geometry, hydrostatic equilibrium, no convective overshooting, and 2 km s^{-1} microturbulence. Starting from these initial estimates, we fixed the effective temperature (T_{eff}) by imposing the excitation equilibrium for Fe I lines. For the microturbulence (ξ), we required no trend of the abundances versus equivalent width (EW) for Fe I lines. Finally, for the surface gravity ($\log g$), we required that ionization equilibrium is achieved between the abundances derived from the Fe I (adopting a non-LTE correction for Fe I of 0.1 dex from; Lind et al. 2012) and Fe II lines. A final iteration of the procedure was made with a model atmosphere computed with these new parameters. The stellar parameters of the two program stars obtained by these procedures are listed in Table 3.

The choice of using a temperature based on the excitation equilibrium (instead of inferred from photometry) ensures that even if the stars were RR-Lyrae stars, for which we have no present indication that they are, the adopted temperature would be relevant for the pulsational phase at which the star was observed (see, e.g., Hansen et al. 2011).

4.2. Line list and equivalent width measurement

We compiled the line lists from Aoki et al. (2007), Hayek et al. (2009), Roederer et al. (2010), Sbordone et al. (2010), and Yong et al. (2013) for the measurements of the atomic absorption lines in the stellar spectra. The log gf values for the Fe II and Ni I lines were taken from Meléndez & Barbuy (2009) and Wood et al. (2014), respectively.
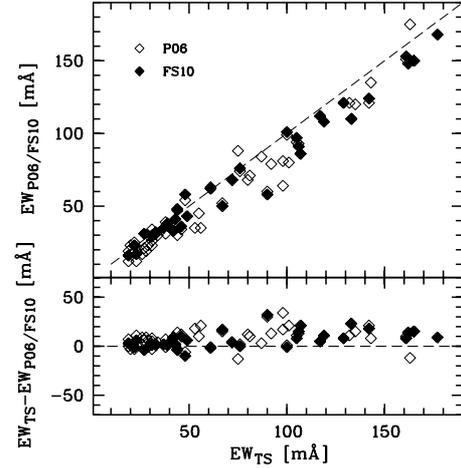

Fig. 2. Comparison of the measured EWs in this study (TS) and in the studies of Preston et al. (2006) and For & Sneden (2010).

Equivalent width measurements were accomplished by fitting a Gaussian profile to the lines simultaneously with a straight-line continuum, where the continuum and line regions were chosen interactively. We compared our EW measurements with those of Preston et al. (2006) and For & Sneden (2010) for CS 22186-005, as seen in Fig. 2. The EWs measured in this study agree with the values obtained in the previous studies. From the EW measurements, abundances were derived using the code WIDTH9 (Sbordone et al. 2004; Kurucz 2005), which uses ATLAS9 model atmospheres to compute line formation in LTE.

4.3. Spectrum synthesis

Line lists that include hyperfine structure (HFS) splitting for Sc, Mn, Co, and Ba were downloaded from Robert Kurucz's web page[3]. Since the EW measurement method is not appropriate for lines where HFS splitting has to be taken into account, we applied the spectrum synthesis method for the Sc, Mn, Co, and Ba lines, producing synthetic spectra with the code SYNTHE (Kurucz 1993b, 2005), and convolving the resulting spectra with a Gaussian profile that includes the broadening effects caused by the instrumental profile and the macroturbulence velocity. The abundances of the species were then adjusted until the observed and synthetic spectra agreed well.

4.4. Uncertainties in abundances

The random (statistical) uncertainties in the elemental abundances were taken to be the standard deviation of individual line measurements (σ) over the square root of the number of lines

---

[3] http://kurucz.harvard.edu/linelists.html

Table 4. Abundances of the species observed in CS 22186-005 and CS 30344-033.

Species	$\log \epsilon_\odot{}^a$		CS 22186-005					CS 30344-033			
		N	$\log \epsilon$	$[X/Fe]$	$[X/Fe]^b$	σ_r	N	$\log \epsilon$	$[X/Fe]$	$[X/Fe]^b$	σ_r
[FeI/H]	7.50	52	4.80	−2.70	···	0.02	83	4.60	−2.90	···	0.01
[FeII/H]	7.50	14	4.95	−2.55	···	0.03	6	4.69	−2.81	···	0.04
Na I	6.30	2	3.57	−0.03	−0.33	0.10	2	3.32	−0.08	−0.28	0.08
Mg I	7.55	5	4.96	0.11	0.31	0.12	6	4.92	0.27	0.57	0.05
Al I	6.46	2	2.81	−0.95	−0.25	0.01	2	2.80	−0.76	−0.06	0.05
Si I	7.54	1	4.61	−0.23	···	0.10	1	4.51	−0.13	···	0.10
Ca I	6.34	5	3.82	0.18	···	0.08	4	3.79	0.35	···	0.03
Sc II^{hfs}	3.07	3	0.51	0.14	···	0.05	8	0.41	0.15	···	0.07
Ti I	4.92	1	2.98	0.76	···	0.10	1	2.62	0.60	···	0.10
Ti II	4.92	18	2.63	0.26	···	0.04	28	2.72	0.61	···	0.03
V II	4.00	···	···	···	···	···	2	1.72	0.53	···	0.04
Cr I	5.65	5	2.80	−0.15	−0.06	0.04	6	2.67	−0.08	0.01	0.04
Cr II	5.65	···	···	···	···	···	1	2.57	−0.27	−0.22	0.10
Mn I^{hfs}	5.50	2	2.38	−0.42	···	0.04	3	2.02	−0.58	···	0.03
Mn II^{hfs}	5.50	···	···	···	···	···	2	2.24	−0.45	···	0.01
Co I^{hfs}	4.91	···	···	···	···	···	4	2.35	0.34	···	0.05
Ni I	6.22	22	3.31	−0.21	···	0.02	12	3.37	0.05	···	0.05
Sr II	2.91	2	−0.78	−1.14	−0.94	0.01	2	−0.61	−0.71	−0.51	0.02
Ba II^{hfs}	2.18	2	−1.24	−0.87	−0.77	0.02	···	···	···	···	···

Notes. [a] Solar abundance ratios are taken from Lodders (2003); [b] The non-LTE abundance ratios.

(N) for each element ($\sigma_r = \sigma/\sqrt{N}$). We adopted an uncertainty of 0.10 dex for species that were measured with spectrum synthesis, or that had only one detected line. This value takes into account the uncertainty in the atomic data and the continuum placement. The random errors are listed in Table 4.

Systematic errors were estimated from the uncertainties in the stellar parameters for each atomic species. The line-to-line scatter of the abundances, which is derived from Fe I lines, is 0.12 for CS 22186-005 and 0.16 for CS 30344-033. We consider as the steepest acceptable slope in the abundance-excitation energy plane a value of $\pm 0.1/N$ per eV (where N is the number of lines). This translates into an uncertainty on $T_{\rm eff}$ of ± 100 K. The abundances derived from the neutral and ionized species are still similar for an uncertainty of ± 0.1 in $\log g$. The abundance-EW slope of the Fe I lines plot is still lower than 0.01 for an uncertainty of ± 0.2 km s^{-1} in ξ. For each model atmosphere, the stellar parameters $T_{\rm eff}$, $\log g$, and ξ were varied within an uncertainty of ± 100 K, ± 0.1 dex, and ± 0.2 km s^{-1}. For example, to estimate the abundance uncertainties arising from the $T_{\rm eff}$, we increased and decreased the value of $T_{\rm eff}$ by 100 K from its original value. We then computed new model atmospheres with these values and re-computed the abundances for each species by fixing the other atmospheric parameters. Then, we compared these abundances with the abundances derived from the original stellar parameters. We applied the same steps for $\log g$ of ± 0.1 dex and ξ of ± 0.2 km s^{-1}. The systematic errors are listed in Table 5.

5. Evolutionary state and masses

The derived effective temperatures and surface gravities of our two program stars unambiguously classify them as HB stars. Their effective temperatures place them close to the red edge of the RR-Lyrae instability strip, whose position and dependence on metallicity is not precisely known (see Preston et al. 2006; For & Sneden 2010, and Sandage 2010 for discussions on this point). This means that they *could* be pulsating RR-Lyrae stars. We inspected the spectra to see if we could detect any sign of

P-Cyg or inverse P-Cyg profiles, which are present in the spectra of RR-Lyraes at some phases, but were unable to detect any. In addition, there is no published hint of photometric variability for either of the stars. Although absence of evidence is not evidence of absence, we assume that both stars are nonvariable red horizontal-branch (RHB) stars. Our derived abundances are expected to be robust even if they are RR-Lyrae stars, since the spectroscopically determined excitation temperature we adopted would be appropriate for the observed phase.

Figure 3 shows evolutionary tracks for HB stars of different mass and $Z = 0.00003$ in the $\log T - \log g$ plane, computed by Cassisi et al. (2004). It is clear from inspection that the tracks are sufficiently well separated in this plane to allow determining the mass of each star. We used the same equation as employed by Preston et al. (2006) to determine $\log g$ from the luminosity[4].

The two black dots in Fig. 3 identify the positions of CS 22186-005 and CS 30344-033 in this plane, with our spectroscopically derived parameters. In their study, Preston et al. (2006) compared their spectroscopic $\log g$ for six RHB stars in the globular cluster M 15, with the log g derived from the magnitudes of the stars, the cluster distance, and an assumed median mass for the HB stars; they called this the "photometric" $\log g$. They derived a linear relation between the photometric and the spectroscopic estimates of $\log g$ [5]. If we use this relation to derive the log g for our program stars, the two stars move toward lower gravities, shown in Fig. 3 as red dots. Adopting the spectroscopic gravities, the two stars should have masses of about 0.75 $M_\odot$ and 0.8 $M_\odot$, and about 0.11 $M_\odot$ lower masses for the "photometric" $\log g$. We refrain from precisely fitting the masses since our derived surface gravity is uncertain by at least a factor of two. Still, this plot provides a useful indication of the masses of the two stars.

---

[4] $\log g = \log(M/M_\odot) + 4\log T_{\rm eff} - \log(L/L_\odot) - 10.607$.

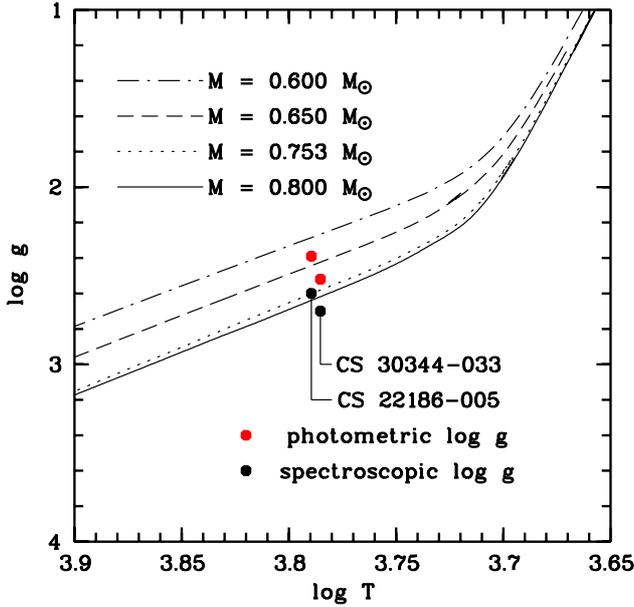[5] $\log g_{\rm phot} = \log g_{\rm spec} + 28.08 - 7.655\log T_{\rm eff}$.

Fig. 3. Evolutionary tracks for HB stars of different masses and metallicity $Z = 0.00003$ in the $\log T - \log g$ plane (Cassisi et al. 2004). The black dots indicate the position of the two stars, with the spectroscopically derived $\log g$, and the red dots correspond to the "photometric" $\log g$, derived from the spectroscopic estimate, according to the empirical calibration of Preston et al. (2006).

6. Abundance results

6.1. The odd-Z elements

We derived abundances for the odd-Z elements Na and Al for CS 22186-005 and CS 30344-033. Sodium abundances were determined for the two target stars from EW measurements, using the 5889 Å and 5895 Å lines. Na I D lines are sensitive to non-LTE effects because of their strengths (Takeda et al. 2003), (Andrievsky et al. 2007). We took into account non-LTE effects of ~-0.3 dex and ~-0.2 dex (Andrievsky et al. 2007) for CS 22186-005 and CS 30344-033. We used the 3944 Å and 3961 Å lines to determine Al abundances of the stars. The 3944 Å line of Al I is generally contaminated by the CH transition, but this contamination is not observable in our spectra. The abundances of aluminium were corrected for a large non-LTE offset of ~0.7 dex, as suggested by Andrievsky et al. (2008) because the aluminium resonance lines are affected by non-LTE effects at low metallicities. The derived light-odd element abundances are listed in Table 4.

6.2. The α-elements

The abundances of the α-elements Mg, Si, Ca, and Ti were computed for our two program stars. For CS 22186-005 the Mg abundances were determined from five Mg I lines (3838 Å, 4702 Å, 5172 Å, 5183 Å, and 5528 Å) and for CS 30344-033 from six lines (3829 Å, 3832 Å, 3838 Å, 5172 Å, 5183 Å, and 5528 Å). The Mg abundances were corrected using the non-LTE effects of ~0.3 dex calculated by Andrievsky et al. (2010). The importance of deviations from LTE for Mg abundance was presented by Andrievsky et al. (2010) in the extended samples of metal-poor stars.

The Si abundances were measured from the 3905 Å line in the spectra of the program stars. This line is sensitive to non-LTE effects, and the effect increases with increasing effective

temperature for metal-poor stars (Shi et al. 2009). The correction that results from the non-LTE effect is ~0.05 dex. We did not take into account this non-LTE effect, because the correction value is lower than the uncertainty on the Si abundance estimates.

To determine Ca abundances, we used five Ca I lines (4226 Å, 4302 Å, 4318 Å, 4454 Å, 6439 Å) for CS 22186-005 and four Ca I lines (4226 Å, 4302 Å, 4318 Å, 4454 Å) for CS 30344-033. The non-LTE effect on the Ca abundances of the program stars was not taken into account (~0.05 dex, given by Spite et al. 2012).

We detected several Ti II lines and only one weak Ti I line in the observed spectra. The differences between the neutral and ionized titanium are [Ti I/Ti II] = 0.36 ± 0.11 for CS 22186-005, and [Ti I/Ti II] = 0.01 ± 0.10 for CS 30344-033.

6.3. The iron-peak elements

We have derived the abundances of the iron-peak elements Sc, V, Cr, Mn, Co, and Ni for CS 30344-033. The abundances of Sc, Cr, Mn, and Ni were determined for CS 22186-005.

We used the Sc II lines 4247 Å, 4314 Å, and 4400 Å to obtain the Sc abundance for CS 22186-005, and eight Sc II lines for CS 30344-033. The effects of HFS were taken into account for all of these lines.

The vanadium abundance is determined from the 3517 Å, and 3556 Å lines of V II for CS 30344-033. We did not find any detectable vanadium line in our spectrum of CS 22186-005.

The Cr abundances were computed from five Cr I lines for CS 22186-005, and from six Cr I lines and one Cr II line (3409 Å) for CS 30344-033. The difference between the neutral and ionized chromium is [Cr I/Cr II] = 0.10 ± 0.11 for CS 30344-033. At low metallicities, the overionization of Cr I causes the deviations from LTE. The abundances of chromium were corrected for a non-LTE effect of ~0.3 dex, taken from Bergemann & Cescutti (2010).

The manganese abundance was measured from three Mn I lines (4030 Å, 4033 Å, 4034 Å) and two Mn II lines (3460 Å, 3488 Å) for CS 30344-033. For CS 22186-005, we determined the Mn abundance from the 4030 Å and 4034 Å Mn I lines. The effects of hyperfine splitting were taken into account for these lines.

We used four Co lines (3405 Å, 3506 Å, 3845 Å, 3894 Å) to measure the Co abundance in the spectrum of CS 30344-033. We accounted for the effect of HFS for Co I lines. We were unable to find any detectable Co line in CS 22186-005.

No Ni I line is confidently detectable in the HARPS spectrum of CS 22186-005. We used the UVES spectrum that covers the UV region, where we measured twenty-two Ni I lines. Twelve Ni I lines were used to obtain the Ni abundance from the spectrum of CS 30344-033.

6.4. The neutron-capture elements

The lines of the neutron-capture elements Sr II (4077 Å and 4215 Å) and Ba II (4554 Å and 4934 Å) were detected in the spectrum of CS 22186-005. We detected only two Sr II lines (4077 Å and 4215 Å) in the spectrum of CS 30344-033. The non-LTE corrections are very important for Ba and Sr at low metallicities (Andrievsky et al. 2009, 2011). To correct the Sr and Ba abundances, we accounted for non-LTE effects of ~0.2 dex and ~0.1 dex from Andrievsky et al. (2011) and Andrievsky et al. (2009), respectively. In addition, the effect of HFS was taken into account for Ba lines, assuming a solar isotopic ratio.

Table 5. Abundance uncertainties due to uncertainties in the atmospheric parameters.

Species	CS 22186-005						CS 30344-033					
	$\Delta T_{\rm eff}$		$\Delta \log g$		$\Delta \xi$		$\Delta T_{\rm eff}$		$\Delta \log g$		$\Delta \xi$	
	[K]		[dex]		[km s^{-1}]		[K]		[dex]		[km s^{-1}]	
	+100	−100	+0.1	−0.1	+0.2	−0.2	+100	−100	+0.1	−0.1	+0.2	−0.2
Na I	−0.07	0.07	0.00	0.00	0.03	−0.03	−0.07	0.07	0.00	0.00	0.03	−0.02
Mg I	−0.06	0.06	0.01	0.00	0.05	−0.05	−0.06	0.07	0.01	−0.01	0.07	−0.07
Al I	−0.08	0.08	0.00	0.00	0.01	−0.01	−0.08	0.08	0.01	0.00	0.02	−0.01
Si I	−0.09	0.08	0.00	0.00	0.04	−0.04	−0.09	0.08	0.00	0.00	0.04	−0.04
Ca I	−0.07	0.06	0.01	0.00	0.03	−0.02	−0.07	0.07	0.00	0.00	0.04	−0.03
Sc II	−0.05	0.06	−0.05	0.03	0.01	−0.01	−0.08	0.07	−0.02	0.03	0.03	−0.02
Ti I	−0.08	0.09	0.00	0.00	0.00	0.00	−0.08	0.09	0.00	−0.01	0.00	0.00
Ti II	−0.05	0.04	−0.03	0.04	0.03	−0.02	−0.06	0.06	−0.03	0.03	0.05	−0.05
V II	⋯	⋯	⋯	⋯	⋯	⋯	−0.07	0.07	−0.02	0.02	0.01	−0.01
Cr I	−0.10	0.09	0.01	0.00	0.01	0.00	−0.10	0.10	0.01	−0.01	0.01	−0.01
Cr II	⋯	⋯	⋯	⋯	⋯	⋯	−0.06	0.06	−0.02	0.02	0.05	−0.04
Mn I	−0.11	0.10	0.01	0.00	0.01	0.00	−0.10	0.11	0.00	−0.01	0.00	−0.01
Mn II	⋯	⋯	⋯	⋯	⋯	⋯	−0.06	0.06	0.01	−0.01	0.03	−0.02
Fe I	−0.09	0.09	0.01	0.00	0.04	−0.03	−0.10	0.10	0.01	0.00	0.05	−0.04
Fe II	−0.02	0.02	−0.03	0.03	0.02	−0.02	−0.01	0.02	−0.04	0.03	0.02	−0.02
Co I	⋯	⋯	⋯	⋯	⋯	⋯	−0.12	0.11	0.01	−0.01	0.01	0.00
Ni I	−0.10	0.10	0.02	−0.02	0.04	−0.04	−0.14	0.14	0.02	−0.02	0.07	−0.06
Sr II	−0.06	0.06	−0.03	0.03	0.02	−0.02	−0.06	0.06	−0.03	0.03	0.04	−0.03
Ba II	−0.07	0.07	−0.03	0.02	0.00	−0.01	⋯	⋯	⋯	⋯	⋯	⋯

7. Discussion

Using high-resolution spectroscopy, we have derived elemental abundance ratios for two very metal-poor HB stars, both of which have derived metallicities lower than [Fe/H] = −2.5.

Our derived atmospheric parameters of CS 22186-005 agree well with those reported in the previous studies of Preston et al. (2006) and For & Sneden (2010). The differences between our measurements and the $T_{\rm eff}$, $\log g$, ξ, and [Fe I/H] of For & Sneden (2010) are 40 K, −0.15 dex, −0.2 km s^{-1}, and −0.05 dex, respectively. Our $T_{\rm eff}$ is lower than the value reported by Preston et al. (2006) by 90 K. We derived a ξ that is higher by 0.3 km s^{-1} than that given by Preston et al. (2006). The $\log g$ and [Fe I/H] in this study are the same as those of Preston et al. (2006).

The abundances of CS 22186-005 generally agree well with the study of For & Sneden (2010), except for Mg and Ti. For the magnesium abundance, For & Sneden (2010) used the two of Mg I b lines: 5172 Å and 5183 Å. We have five Mg lines, which include the two Mg I b lines. If we use only the two Mg lines, our Mg abundance agrees well with the value reported by For & Sneden (2010). This shows that, as expected, the different Mg abundances are due to the lines used during the analysis. Our Ti abundance of CS 22186-005, derived from 18 Ti II lines, agrees reasonably well with the metal-poor halo stars, although it is somewhat higher than those of the previous studies. We show a comparison the abundance ratios of CS 22186-005 with those of the previous studies in Fig. 4.

In general, the abundance ratios that we report here follow the Galactic trends traced by RGB and TO stars (Yong et al. 2013; Roederer et al. 2014b), confirming previous claims that HB stars are indeed reliable tracers of Galactic chemical evolution.
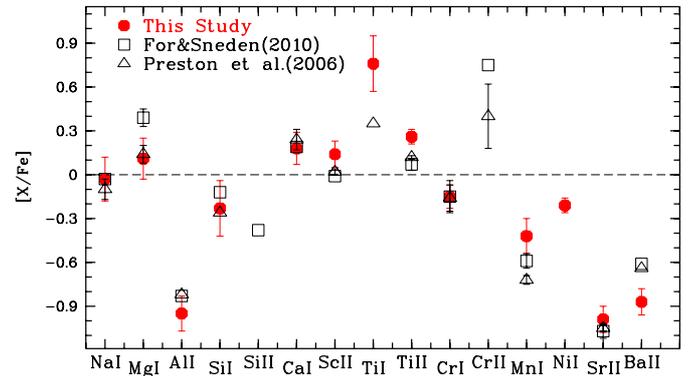

Fig. 4. Comparison for CS 22186-005 of the abundance ratios derived from this analysis with the previous studies of Preston et al. (2006) and For & Sneden (2010). The error bars show the random uncertainties in the abundance ratios.

7.1. The odd-Z elements

The abundances of the odd-Z elements Na and Al decrease with decreasing metallicity. The amount of Na and Al depends on the neutron excess, which is produced in the CNO cyle during He burning (Kobayashi et al. 2006). We show [(Na, Al)/Fe] vs. [Fe/H] in Fig. 5. The Na and Al abundance ratios of our target stars are compatible with the trend of the other metal-poor stars (Yong et al. 2013).

7.2. The α-elements

Generally, metal-poor stars are enriched in α-elements, because of the lack of the contribution of Type Ia at these metallicities. As expected, the Mg, Ca, and Ti abundance ratios to iron of our target stars are overabundant with respect to the solar values. However, the Si abundance ratios of both target
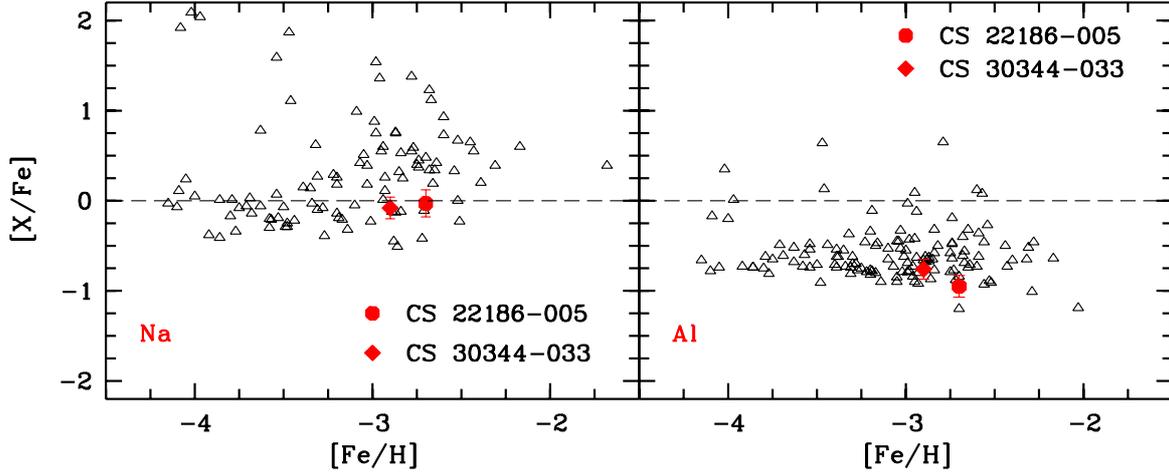
Fig. 5. Light-odd elements (Na and Al) abundance ratios as a function of [Fe/H]. Open triangles show the Galactic giant and turnoff stars (Yong et al. 2013). The error bars show the random errors for each program star.

stars are underabundant with respect to the solar values. For CS 22816-005, our measurement confirms those of Preston et al. (2006) and For & Sneden (2010). These abundance values are lower than the general trend, as shown in Fig. 6. We stress that the Si abundance is based on a single line, the 3906 Å line, as is the case in other very metal-poor RHB and TO stars.

7.3. The iron-peak elements

Sc abundance for the metal-poor stars follow a slightly decreasing trend with metallicity, as shown in Fig. 7. The abundance results of Sc for our samples are compatible with the observed trend of this element. The V abundance, derived from single ionized vanadium, of CS 30344-033 is 0.53 ± 0.04. These overabundances in the vanadium abundance are unreliable because of the unresolved blends in the UV spectral range (Barklem et al. 2005). The metal-poor stars exhibit underabundances of Cr and Mn with decreasing metallicity (Cayrel et al. 2004; Lai et al. 2008). Roederer et al. (2014b) presented the trend of Cr and Mn abundances for subgiant, red giant, main-sequence, and HB stars. The Mn abundances of HB stars decrease with decreasing temperature. The chromium abundances are close to zero for the higher temperatures, while they decrease with decreasing temperature. Our HB samples almost agree with this trend of Cr and Mn. The [Co/Fe] displays an increase with decreasing metallicity (Cayrel et al. 2004). The cobalt abundance of 0.34 ± 0.05 agrees with the observed trend, as seen in Fig. 7.

7.3.1. Evidence for scatter in [Ni/Fe]?

The [Ni/Fe] for CS 22186-005 was determined here for the first time. The value [Ni/Fe] = -0.21 ± 0.02 was determined from 22 lines in the UV range. From Fig. 7 it can be appreciated that although the general trend with [Fe/H] is constant, [Ni/Fe] = 0.0, as expected for elements with the same nucleosynthetic origin, the scatter around this value is quite large. If we only consider the Ni abundances in the 38 stars analyzed by Yong et al. (2013), neglecting the data re-analyzed from the literature, the scatter in [Ni/Fe] is 0.2 dex much larger than what is expected from the errors in the individual measurements. If we consider the whole sample of 190 stars of Yong et al. (2013), which we took as comparison sample, the scatter is 0.17 dex. This scatter is higher than that in other samples of metal-poor stars. For example, in the

sample of Bonifacio et al. (2009) it is only of 0.06 dex, and in the large sample of Roederer et al. (2014b) it is only 0.10 dex. This raises the question if the scatter in [Ni/Fe] is real. Our measurement of Ni in CS 22186-005 is almost a factor of two below the mean of the rest of the sample.

In the sample of HB stars of For & Sneden (2010) there are three BHB stars (HD 60778, HD 74721, HD 93329) for which Ni could be measured only from Ni II lines, and they imply [Ni/Fe] between –0.4 and –0.3. Other metal-poor stars that have [Ni/Fe] ≤ −0.2 are in the sample of Roederer et al. (2014b) CS 22174-020 and CS 22964-183, in the sample of Yong et al. (2013) we find CS 22953-037, CS 31061-032, CS 22169-035, HE 1012-1540, HD 186478, HE 2232-0603, CS 29499-060, HE 1207-3108, and HE 2142-5656.

Among HB stars are a few stars in the sample of For & Sneden (2010) with [Ni/Fe] considerably higher than the mean (CS 22878-121, CS 22940-70, CS 22948-006, CS 22944-039, CS 22951-077, and CS 22886-043). The mean [Ni/Fe] of these stars is +0.53, with an r.m.s scatter of 0.13 dex. We point out that there are three stars with high [Ni/Fe] in the sample of TO stars of Bonifacio et al. (2012), in particular SDSS J082521+040334, with [Ni/Fe] = +0.48, measured from four Ni I lines, but also SDSS J233113-010933, SDSS J230814-085526, SDSS J154246+054426, and SDSS J113528+010848, which span the range +0.21 to +0.32 in [Ni/Fe], all from several Ni I lines. Furthermore, Cohen et al. (2013) reported that the Ni abundance ratios of HE 1422-0818, HE 1434-1442, HE 0411-5725, and HE 1320+0139 have a range of +0.42 to +0.76. Two stars (CS 22943-137 and G004-036) with high [Ni/Fe] were discovered by Roederer et al. (2014b). The nickel abundance ratio of G004-036 was derived from eight lines as [Ni/Fe] = +0.57 ± 0.11. Finally, in the full sample of Yong et al. (2013) nine stars have [Ni/Fe] ≥ +0.3: CS 30339-069, CS 29518-043, HE 1424-0241, CS 22948-093, CD −24° 17504, HE 0049-3948, HE 0228-4047, HE 1506-0113, and HE 2247-7400.

Is this span of a factor of three in [Ni/Fe] real? The data ought to be analyzed in more detail before a firm conclusion on this question can be reached. It is perhaps sobering to note that the most Ni-rich star in the sample of Yong et al. (2013), CS 29518-043, with [Ni/Fe] = +0.63, is a reanalysis of the equivalent widths of Bonifacio et al. (2009), who derived [Ni/Fe] = +0.07. In addition, for CS 30339-069 and CS 22948-093, Yong et al. (2013) derived [Ni/Fe] ratios much
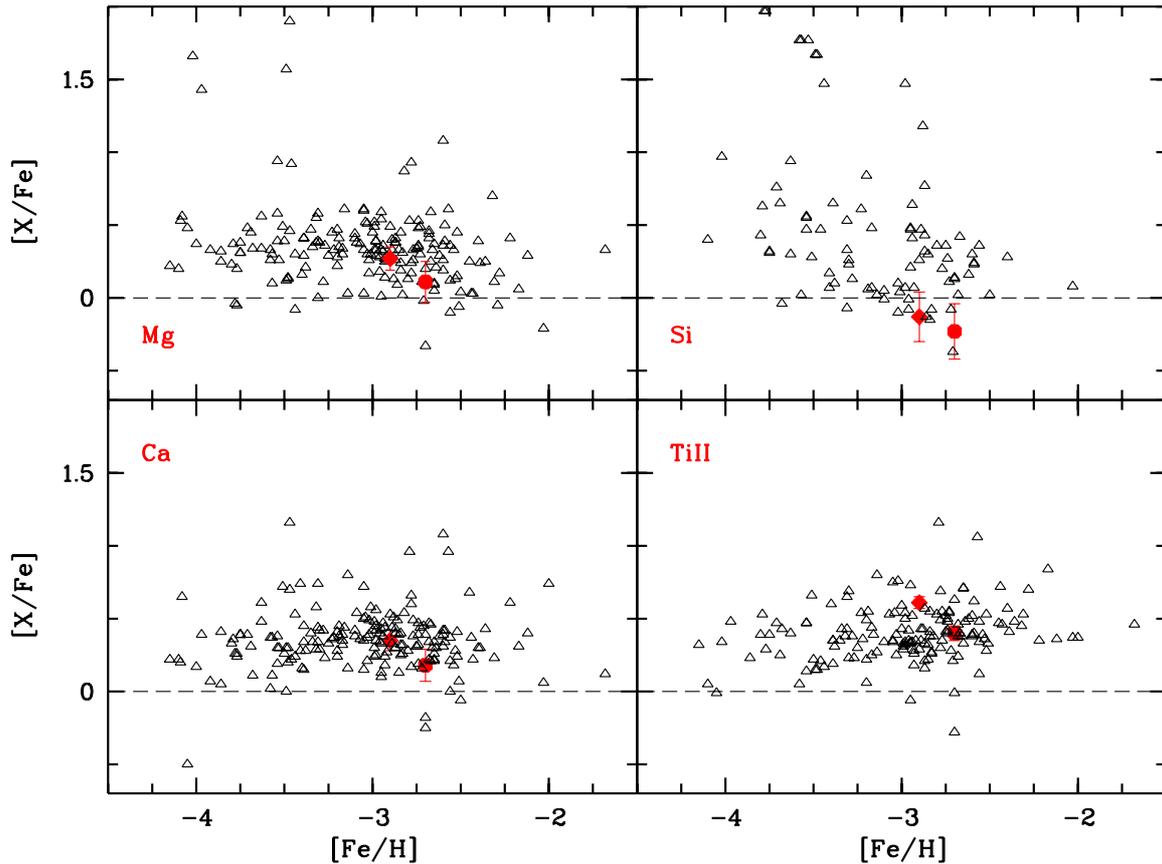
Fig. 6. α-element (Mg, Si, Ca, Ti) abundance ratios of the program stars, compared with the Galactic trend. Symbols and references are the same as in Fig. 5.

higher than those derived by Bonifacio et al. (2009) from the same equivalent widths. On the side of low [Ni/Fe] stars in the sample of Yong et al. (2013) for CS 29499-060, they provide [Ni/Fe] = −0.21, while Bonifacio et al. (2009) provide +0.19, for CS 22953-037 Yong et al. (2013) give [Ni/Fe] = −0.37, while Bonifacio et al. (2009) give +0.04 and for CS 31061-032 Yong et al. (2013) give −0.34, while Bonifacio et al. (2009) give +0.03. A homogeneous reanalysis of the available data is necessary before a firm conclusion on the reality of the scatter in [Ni/Fe] can be drawn.

7.4. The neutron-capture elements

We determined the abundances of the light and heavy neutron-capture elements Sr and Ba for CS 22186-005, while we only determined the Sr abundance for CS 30344-033. In both our HB stars the ratios of Sr and Ba to iron are lower than solar, which is not unusual among metal-poor stars. In Fig. 8, we compare the [Sr, Ba/Fe] abundance ratios as a function of [Fe/H] for our stars with those of the other metal-poor stars. The barium abundance of CS 22186-005 and strontium abundance of CS 30344-033 follow the general trend that decreases with decreasing metallicity, although both are on the low side.

Based on the pioneering observations of Spite & Spite (1978), Truran (1981) suggested that in low-metallicity stars all the neutron-capture elements are formed by the r-process[6]. However, two decades later, it became clear that this view might

be too simplistic. Travaglio et al. (2004) concluded that although the classic s-process[7] could not account for the observations of Sr, Y, Zr and their ratios to heavy neutron-capture elements (Ba, Eu), neither was the r-process acting alone. They thus suggested that Sr, Y, and Zr are formed via s-process in low-metallicity massive stars and called this process lighter element primary process (LEPP). François et al. (2007) noted that Sr, Y, and Zr exhibit an overabundance compared with Ba for metal-poor stars. Sneden et al. (2008) showed that the [Ba/Sr] abundance ratio increases as the [Ba/Fe] ratio increases. Roederer et al. (2014a) noted that two of their sample stars (CS 22891-200 and HE 1012-1540) had [Ba/Sr] > 0, and noted that the ratios are consistent with the 16 metal-poor stars of Sneden et al. (2008) that were enhanced by r-process nucleosynthesis. We show the [Ba/Sr] ratio (heavy/light) versus [Ba/Fe] for CS 22186-005 and the other metal-poor stars in Fig. 9.

As reported by For & Sneden (2010) and Preston et al. (2006), CS 22186-005 has a high [Ba/Sr] and low [Ba/Fe] ratio. Although this abundance pattern is exceptional among HB stars, among the extremely metal-poor giants of François et al. (2007) many exhibit similar ratios. The [Ba/Sr] ratios in CS 22186-005 was interpreted by For & Sneden (2010) as evidence for a multiplicity of neutron-capture synthesis processes.

---

[6] Rapid neutron-capture, i.e., the time between successive captures of neutrons is shorter than with respect to the time for β decay.

[7] Slow neutron-capture, i.e., the time between neutron-captures is longer than the time for β decays. The classic s-process comprises the main s-process, responsible for the bulk of the light neutron-capture elements in the solar system and the weak s-process, characterized by a high neutron-to-seed nuclei ratios, this process takes place in metal-poor stars.
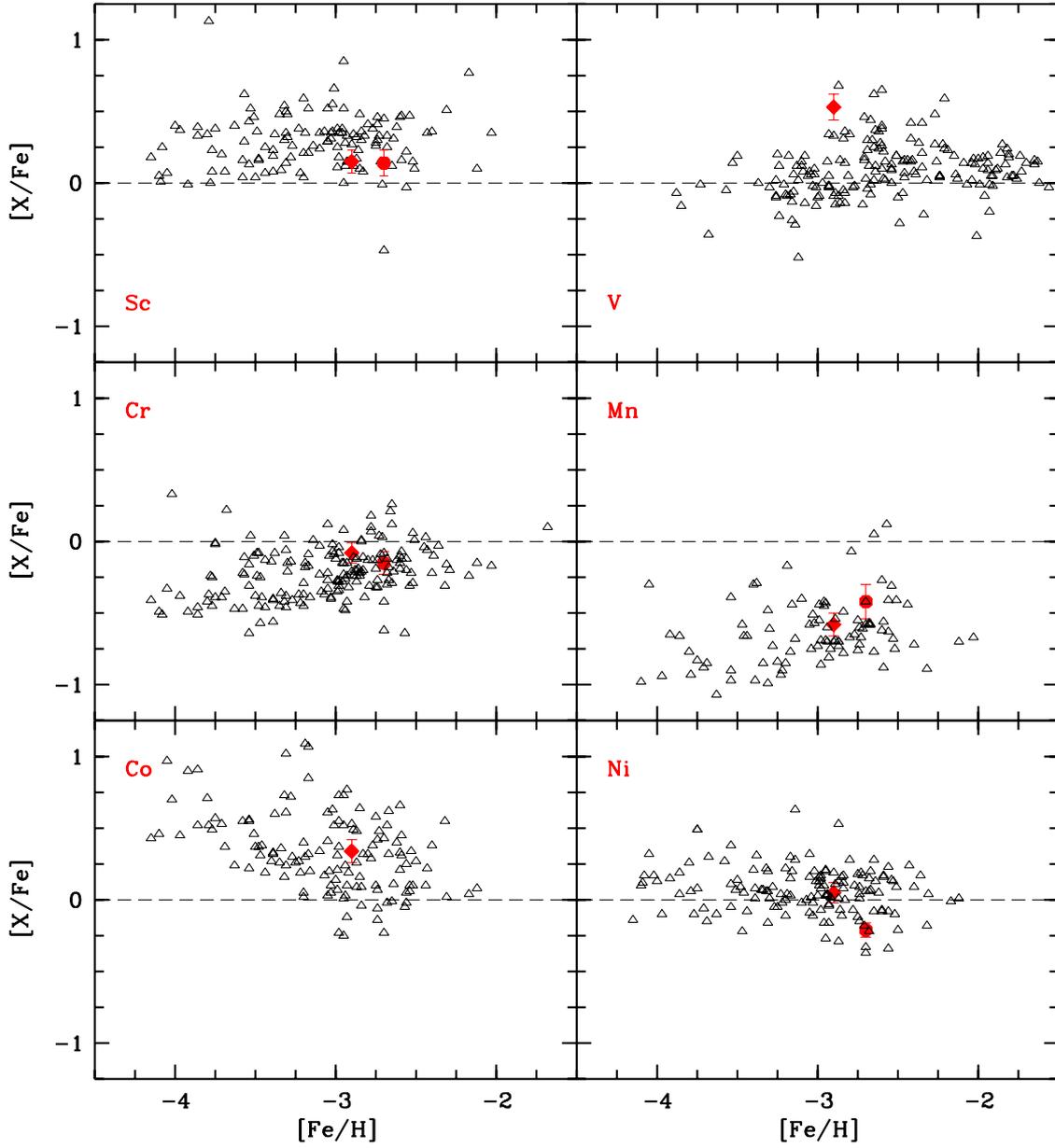
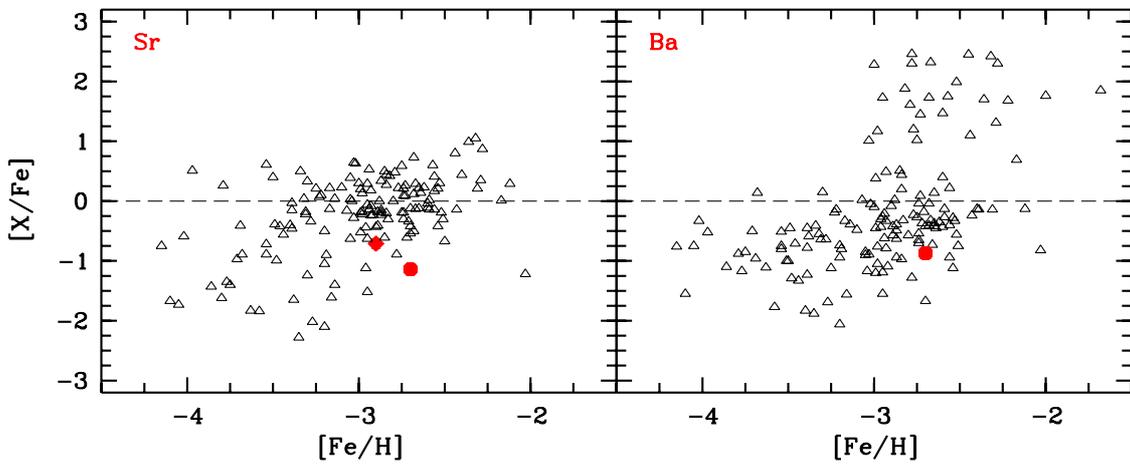**Fig. 7.** [Sc, Cr, Mn, Co, Ni/Fe] vs. [Fe/H]. Symbols and references are the same as in Fig. 5.

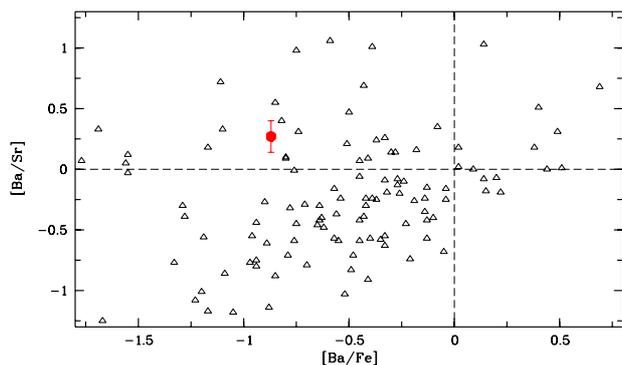**Fig. 8.** [Ba, Sr/Fe] vs. [Fe/H]. Symbols and references are the same as in Fig. 5.

Fig. 9. [Ba/Sr] vs. [Ba/Fe]. Symbols and references are the same as in Fig. 5.

8. Conclusions

Our analysis, based on original spectra of the newly discovered HB metal-poor star CS 30344-033 and of the already known HB star CS 22186-005 confirmed that HB stars are reliable tracers of the Galactic chemical evolution. Their higher luminosity, with respect to turnoff stars, makes them suitable for probing the halo system of the Galaxy at larger distances.

The Ni abundance in CS 22186-005, determined here for the first time, implies a [Ni/Fe] significantly below the mean value for most metal-poor stars. A closer inspection of the literature data suggests that taking the data at face value, there might be room for an intrinsic scatter in the [Ni/Fe] ratios, but the large discrepancies in the [Ni/Fe] determinations in the same stars by different authors implies that it is too early to draw a firm conclusion on this question.

Our radial velocity measurements for CS 22186-005, together with the measurement of Preston et al. (2006), imply that this star is a radial velocity variable. More observations are needed to confirm this variability.

References

Andrievsky, S. M., Spite, M., Korotin, S. A., et al. 2007, A&A, 464, 1081
Andrievsky, S. M., Spite, M., Korotin, S. A., et al. 2008, A&A, 481, 481
Andrievsky, S. M., Spite, M., Korotin, S. A., et al. 2009, A&A, 494, 1083
Andrievsky, S. M., Spite, M., Korotin, S. A., et al. 2010, A&A, 509, A88
Andrievsky, S. M., Spite, F., Korotin, S. A., et al. 2011, A&A, 530, A105
Aoki, W., Beers, T. C., Christlieb, N., et al. 2007, ApJ, 655, 492
Barklem, P. S., Christlieb, N., Beers, T. C., et al. 2005, A&A, 439, 129
Beers, T. C., Preston, G. W., & Shectman, S. A. 1992, AJ, 103, 1987
Beers, T. C., Chiba, M., Yoshii, Y., et al. 2000, AJ, 119, 2866
Bergemann, M., & Cescutti, G. 2010, A&A, 522, A9
Bonifacio, P., Spite, M., Cayrel, R., et al. 2009, A&A, 501, 519
Bonifacio, P., Sbordone, L., Caffau, E., et al. 2012, A&A, 542, A87
Casagrande, L., Ramírez, I., Meléndez, J., Bessell, M., & Asplund, M. 2010, A&A, 512, A54
Cassisi, S., Castellani, M., Caputo, F., & Castellani, V. 2004, A&A, 426, 641
Castelli, F., & Kurucz, R. L. 2003, in Modelling of Stellar Atmospheres, eds. N. Piskunov, W. W. Weiss, & D. F. Gray, IAU Symp., 210, A20
Cayrel, R., Depagne, E., Spite, M., et al. 2004, A&A, 416, 1117
Christlieb, N., Schörck, T., Frebel, A., et al. 2008, A&A, 484, 721
Cohen, J. G., Christlieb, N., Thompson, I., et al. 2013, ApJ, 778, 56
Dekker, H., D'Odorico, S., Kaufer, A., Delabre, B., & Kotzlowski, H. 2000, in Optical and IR Telescope Instrumentation and Detectors, eds. M. Iye, & A. F. Moorwood, SPIE Conf. Ser., 4008, 534
For, B.-Q., & Sneden, C. 2010, AJ, 140, 1694
For, B.-Q., Sneden, C., & Preston, G. W. 2011, ApJS, 197, 29
François, P., Depagne, E., Hill, V., et al. 2007, A&A, 476, 935
Hansen, C. J., Nordström, B., Bonifacio, P., et al. 2011, A&A, 527, A65
Hattori, K., Yoshii, Y., Beers, T. C., Carollo, D., & Lee, Y. S. 2014, ApJ, 784, 153
Hayek, W., Wiesendahl, U., Christlieb, N., et al. 2009, A&A, 504, 511
Kobayashi, C., Umeda, H., Nomoto, K., Tominaga, N., & Ohkubo, T. 2006, ApJ, 653, 1145
Kurucz, R. 1993a, ATLAS9 Stellar Atmosphere Programs and 2 km s^{-1} grid, Kurucz CD-ROM No.13 (Cambridge, Mass.: Smithsonian Astrophysical Observatory)
Kurucz, R. 1993b, SYNTHE Spectrum Synthesis Programs and Line Data, Kurucz CD-ROM No. 18 (Cambridge, Mass.: Smithsonian Astrophysical Observatory)
Kurucz, R. L. 2005, MmSAI Suppl., 8, 14
Lai, D. K., Bolte, M., Johnson, J. A., et al. 2008, ApJ, 681, 1524
Lind, K., Bergemann, M., & Asplund, M. 2012, MNRAS, 427, 50
Lodders, K. 2003, ApJ, 591, 1220
Meléndez, J., & Barbuy, B. 2009, A&A, 497, 611
Norris, J. E., Ryan, S. G., & Beers, T. C. 1996, ApJS, 107, 391
Norris, J. E., Ryan, S. G., & Beers, T. C. 1999, ApJS, 123, 639
Preston, G. W., Sneden, C., Thompson, I. B., Shectman, S. A., & Burley, G. S. 2006, AJ, 132, 85
Roederer, I. U., Sneden, C., Thompson, I. B., Preston, G. W., & Shectman, S. A. 2010, ApJ, 711, 573
Roederer, I. U., Preston, G. W., Thompson, I. B., Shectman, S. A., & Sneden, C. 2014a, ApJ, 784, 158
Roederer, I. U., Preston, G. W., Thompson, I. B., et al. 2014b, AJ, 147, 136
Sandage, A. 2010, ApJ, 722, 79
Sbordone, L., Bonifacio, P., Castelli, F., & Kurucz, R. L. 2004, MmSAI Suppl., 5, 93
Sbordone, L., Bonifacio, P., Caffau, E., et al. 2010, A&A, 522, A26
Shi, J. R., Gehren, T., Mashonkina, L., & Zhao, G. 2009, A&A, 503, 533
Sneden, C., Cowan, J. J., & Gallino, R. 2008, ARA&A, 46, 241
Spite, M., & Spite, F. 1978, A&A, 67, 23
Spite, M., Andrievsky, S. M., Spite, F., et al. 2012, A&A, 541, A143
Takeda, Y., Zhao, G., Takada-Hidai, M., et al. 2003, ChJAA, 3, 316
Travaglio, C., Gallino, R., Arnone, E., et al. 2004, ApJ, 601, 864
Truran, J. W. 1981, A&A, 97, 391
Wood, M. P., Lawler, J. E., Sneden, C., & Cowan, J. J. 2014, ApJS, 211, 20
Yi, S. K., Kim, Y.-C., & Demarque, P. 2003, ApJS, 144, 259
Yong, D., Norris, J. E., Bessell, M. S., et al. 2013, ApJ, 762, 26